Journal of Rock Mechanics and Geotechnical Engineering 9 (2017) 611–622

Contents lists available at ScienceDirect

Journal of Rock Mechanics and Geotechnical Engineering

journal homepage: www.rockgeotech.org

Full Length Article

Hard rock tunnel boring machine penetration test as an indicator of chipping process efficiency

M.C. Villeneuve*

Department of Geological Sciences, University of Canterbury, Christchurch, 8140, New Zealand

ARTICLE INFO

Article history:
Received 16 September 2016
Received in revised form
13 November 2016
Accepted 2 December 2016
Available online 1 August 2017

Keywords:
Penetration rate
Grinding
Chipping
Geological characteristics
Face stability

ABSTRACT

The transition from grinding to chipping can be observed in tunnel boring machine (TBM) penetration test data by plotting the penetration rate (distance/revolution) against the net cutter thrust (force per cutter) over the full range of penetration rates in the test. Correlating penetration test data to the geological and geomechanical characteristics of rock masses through which a penetration test is conducted provides the ability to reveal the efficiency of the chipping process in response to changing geological conditions. Penetration test data can also be used to identify stress-induced tunnel face instability. This research shows that the strength of the rock is an important parameter for controlling how much net cutter thrust is required to transition from grinding to chipping. It also shows that the geological characteristics of a rock will determine how efficient chipping occurs once it has begun. In particular, geological characteristics that lead to efficient fracture propagation, such as fabric and mica contents, will lead to efficient chipping. These findings will enable a better correlation between TBM performance and geological conditions for use in TBM design, as a basis for contractual payments where penetration rate dominates the excavation cycle and in further academic investigations into the TBM excavation process.

1. Introduction

It is generally accepted that during hard rock tunnel boring machine (TBM) excavation, a cutter first creates a crushed zone at the cutter-rock interface and the stresses from the thrust of the cutter are transmitted through this crushed zone into the adjacent undamaged rock (Snowdon et al., 1982; Bruland, 1998; Cigla et al., 2001; Zhang, 2001; Rostami et al., 2002). The induced stresses and dilation within the crushed zone cause tensile fracturing of rock away from the crushed zone. Eventually, fractures generated by subsequent cutter passes extend either to the rock surface or to the fractures propagating from adjoining kerfs and coalesce to form chips. This occurs at different cutter thrust magnitudes for different rock types. If the cutter thrust necessary for tensile fracture propagation is not achieved, due to excessively high cutter thrust requirements or an underpowered TBM, then only grinding at the crushed zone occurs. Grinding produces only fines, rather than chips, leading to much lower penetration rate. Chipping is a more efficient excavation process because generating chips through tensile fracturing is much more efficient than the formation of fines in the crushed zone (Teale, 1964; Snowdon et al., 1982; Bruland, 1998; Gertsch et al., 2007; Yin et al., 2014). The formation of chips by the chipping process is therefore critical for achieving high penetration rates.

Endeavours to develop penetration rate prediction formulas using net cutter thrust for intact rock (Robbins, 1970; Bruland, 1998) and jointed rock masses (Barton, 2000; Bieniawski et al., 2006; Sapigni et al., 2002) demonstrate the value of analytical methods to predict penetration rate for design and performance assessment. Maidl et al. (2008) showed that weaker rocks required lower thrust to achieve the same penetration rate as stronger rocks using a penetration rate versus thrust schematic loosely based on Robbins (1970). Recently, several prediction models have also been proposed to determine relationships between TBM performance and rock mass characteristics (Sapigni et al., 2002; Alber, 2008; Gong and Zhao, 2009; Hassanpour et al., 2011; Farrokh et al., 2012).

This research explores what TBM penetration testing can show the excavation process. Based on the early works by Villeneuve (2008) and Frenzel et al. (2012), penetration tests are defined

* Fax: +64 3 364 2769.
E-mail address: marlene.villeneuve@canterbury.ac.nz.

Peer review under responsibility of Institute of Rock and Soil Mechanics, Chinese Academy of Sciences.

http://dx.doi.org/10.1016/j.jrmge.2016.12.008

and corresponding values are demonstrated for TBM performance analysis. Geological characteristics are linked to the chipping process identified with the penetration tests. TBM operational data and results from penetration tests are analysed to provide feedback to TBM operators about whether excavation is occurring efficiently through chipping or inefficiently through grinding. Then TBM penetration test results are used to identify areas of stress-induced face instability. Finally, TBM penetration test data are demonstrated for further understanding of relationships between rock strength, geological characteristics and chipping process.

2. Methods and materials

2.1. Penetration test methodology

We performed a total of 16 penetration tests in three different rock units in the Swiss Alps: schist, granite and gneiss, using three Herrenknecht hard rock gripper TBMs with a range of 8.83–9.58 m in diameter. All TBMs utilised 432 mm diameter cutters with 90 mm spacing on centre. During normal TBM start-up, only a few data points at low penetration rates were recorded by the data acquisition system (DAS) due to the sampling interval (typically 0.1 s). In order to capture sufficient data through the full range of penetration rates, penetration tests were adopted (Villeneuve, 2008; later described in detail in Frenzel et al., 2012), and conducted by gradually increasing the TBM thrust from full stop to the maximum thrust over a period of 8–10 min. The cutterhead rotational speed (RPM) was kept constant during these tests, typically ranging from 5.5 rpm to 6.2 rpm, and was selected based on the face condition (i.e. it would be higher in stable face conditions than that in blocky face conditions). Depending on the operator, RPM and rock type, the length of tunnel tested is approximately 30–200 mm.

The penetration rate (mm/rev) is used in this investigation, rather than speed (mm/min), because this removes the effect of RPM and allows comparison of test results from different strokes. The thrust value obtained from the DAS is gross thrust, which is the amount of force exerted by the thrust pistons. This thrust incorporates friction on the TBM head, which is independent of cutting processes occurring at the tunnel face. The net cutter thrust is used, which is the gross thrust minus the frictional losses, divided by the number of cutters, to allow comparison of test results from different locations and different TBMs. The friction contribution to gross thrust is estimated by averaging the gross thrust required to reverse and advance the TBM cutterhead (i.e. moving the cutterhead when it is not touching the rock at the face, usually during cutter changes). The gross thrust also includes the impacts of TBM stiffness and the losses in the hydraulic systems, but these should remain constant for any TBM.

2.2. Geological materials

At test locations, geological and geomechanical data were collected from the exposed rock walls, the chips on the conveyor system and through exploratory core drilling ahead of the tunnel face. Lithology and rock mass characteristics were recorded by mapping the tunnel walls, logging the core, when available, and collecting chips and wall samples at regular intervals. Each rock unit was encountered over a tunnel length of hundreds of metres and has variability at the metre to tens of metres scale in terms of mineralogy, grain size and fabric. These investigations were conducted in unweathered, massive rock masses (Fig. 1a–c) in order to focus on the relationship between intact rock strength and rock cutting process. In these rock masses, TBM performance is dominated by intact rock fracturing processes, rather than rock mass failure processes associated with pre-existing fractures and joints, such as those reported in Sapigni et al. (2002) and Hassanpour et al. (2011, 2015). Due to the tunnel depth (1800–2500 m), the stresses in the face commonly led to spalling and face instability (Fig. 1d), which was not necessarily associated with spalling in the walls (note the cutter kerfs in the gauge area of the face shown in the upper right corner of Fig. 1d).

The schist and granite in this study are generally foliated, with varying intensities of schistosity (Fig. 2a, c and d). Foliation, when present, is consistently dipping steeply and nearly parallel to the tunnel face, with spacing at the scale of tens to hundreds of millimetres. The gneiss in this study has banding (Fig. 2b), which is subhorizontal, with spacing also at the scale of tens to hundreds of millimetres. All of the lithologies are typically composed of quartz, potassium-feldspar, plagioclase and micas, with minor components of alteration minerals, such as chlorite, sericite and pyrite (Villeneuve, 2008). The mineral composition of the schist is typically 25–30% quartz, 50% feldspar and 25–35% mica. More micacious sections of the schist contain 30% quartz, 30% feldspar and 40% mica. The average quartz content in the granite is 30%, with feldspar content around 50% and mica content around 20%. Some less foliated sections contain around 50% quartz, nearly 50% feldspar and less than 5% mica. More micacious sections of the granite contain less than 15% quartz, nearly 50% feldspar and over 40% mica. The mineral composition of the gneiss is typically 35% quartz, 55% feldspar and less than 10% mica.

Point load index strength tests were performed on cores sampled ahead of the tunnel face in the granite. If such cores were not available, uniaxial compressive strength (UCS) was obtained from cores sampled and tested by the contractor from tunnel walls in the schist and granite (Table 1). No strength values are available for the tests in the gneiss. The UCS results did not include elastic modulus or tensile strength. Uniaxial compression tests were not always conducted on samples from the same locations as the penetration tests. Thin section analyses of rocks from uniaxial compression test locations and penetration test locations were utilised to select the most appropriate UCS value (if there were several UCS values near a penetration test site). For Granite 4, the nearest UCS values do not correspond to the lithology encountered during the test so the point load index strength value from a sample at the test location was converted to UCS according to the ratio of point load index strength to UCS for that lithology derived in Villeneuve (2008).

3. Penetration test results in Alpine schist, granite and gneiss

The penetration rate and net cutter thrust data from a penetration test are plotted against each other to obtain a penetration curve for each test, as shown in Figs. 3–5.

The common logarithms of both penetration rate and net cutter thrust can be plotted (Figs. 6–8) to derive the penetration coefficient (PC) and critical thrust (M_1, in kN) to obtain the penetration rate of 1 mm/rev as defined by Bruland (1998). The linear regression of the logarithm curves is defined by Bruland (1998) as

$$\log_{10} i_0 = A_R \log_{10} M_1 + B_R \quad (1)$$

where i_0 is the penetration rate, and A_R and B_R are the regression constants (as indicated in Figs. 6–8). Bruland (1998) showed that PC is equal to A_R, while M_1 can be found by solving Eq. (1) for $i_0 = 1$ mm/rev. The values of PC (or A_R), B_R, and M_1 for the penetration tests obtained in this study and those from two marble samples tested in Yin et al. (2014) and one granite sample tested in Gong et al. (2007) are given in Table 2.

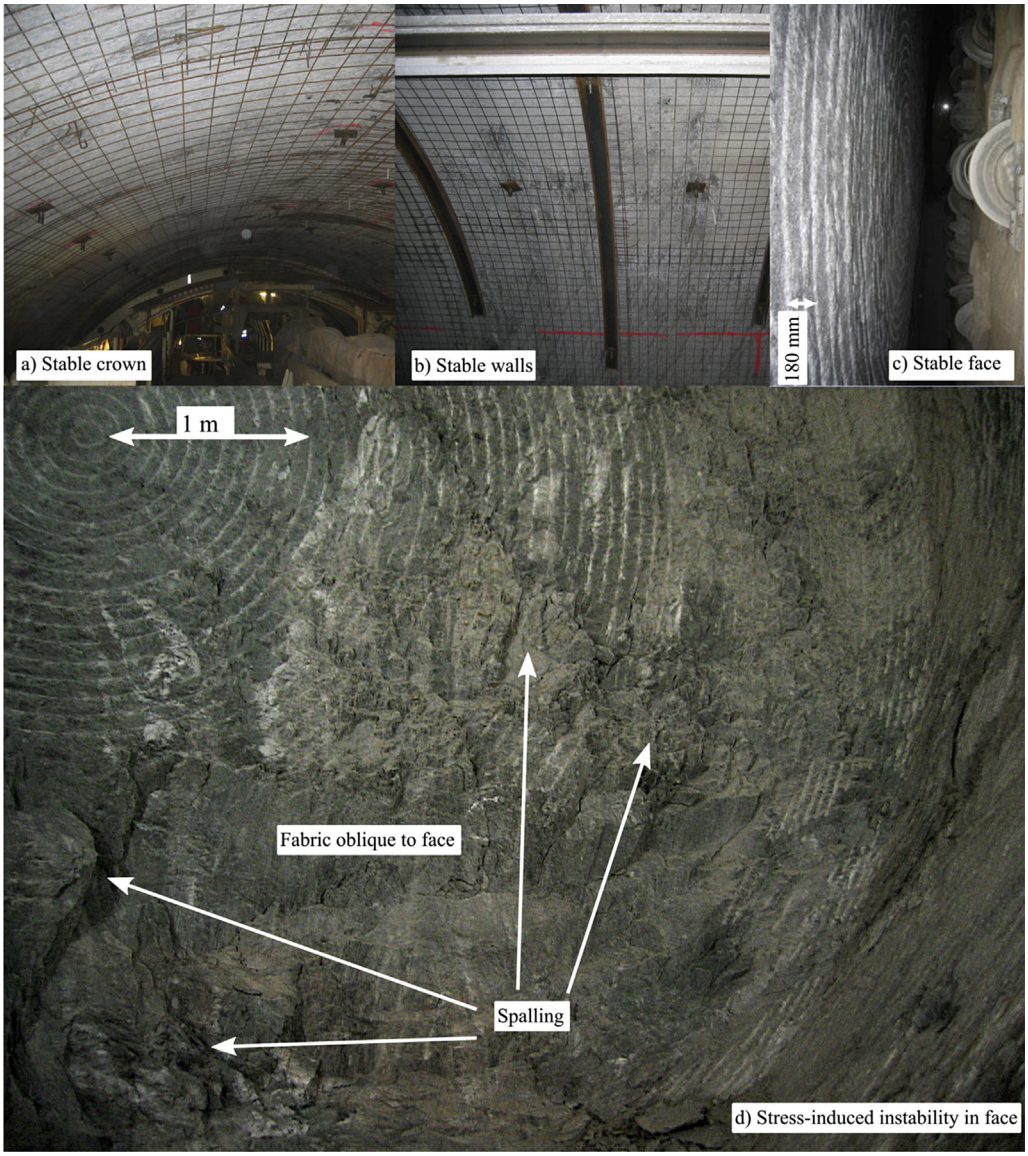

Fig. 1. Conditions of rock masses in which penetration tests were conducted. The rock masses were massive, without sign of crown (a) or wall (b) instability due to fracturing. In many tests, the face was stable and all kerfs were visible (c). In some cases, the face experienced spalling, which led to stress-induced face instability (d) despite occurring in massive rock (no or few joints).

The penetration index (field penetration index in Farrokh et al. (2012), and boreability index in Gong et al. (2007)), which is the ratio of the net thrust to the penetration rate, can be plotted against the penetration rate (Figs. 9 and 10). The curves follow a power law with the following form:

$$PI = SRMBI(i_0)^{-c} \quad (2)$$

where PI is the penetration index (kN (rev mm^{-1})$^{-1}$), $SRMBI$ is the specific rock mass boreability index (Gong et al., 2007), and $-c$ is a fitting parameter. $SRMBI$ is the penetration index at a penetration rate of 1 mm/rev. Gong et al. (2007) and Yin et al. (2014) argued that $-c$ should be approximately 0.75, and the results from our tests show that $-c$ ranges from 0.595 to 0.9, with an average of 0.76. The values of $SRMBI$ and $-c$ for the penetration tests obtained in this study and those from two marble samples in Yin et al. (2014) and one granite sample in Gong et al. (2007) are also given in Table 2.

4. Analyses of penetration test results

4.1. Penetration curves

Penetration curves (Fig. 11) can highlight: (1) the minimum thrust required to begin advancing the TBM; (2) the initial penetration behaviour dominated by grinding (creating fines); (3) the change from grinding to chipping (creating chips), called the critical thrust (Robbins, 1970), located at the inflection point; (4) the chipping efficiency represented by the slope of the line past the inflection point; and (5) the point of steady-state penetration.

The minimum thrust and grinding portion of the curve will depend on the resistance of the rock to crushing. The critical thrust point and the slope of the curve during chipping (as discussed in Samuel and Seow (1984), Zhang et al. (2003) and Gehring (2009)), are related to rock strength, brittleness, mineralogy and fabric (Villeneuve et al., 2007, 2012; Villeneuve, 2008), and the stress at the tunnel face (Yin et al., 2014). The location of the critical thrust

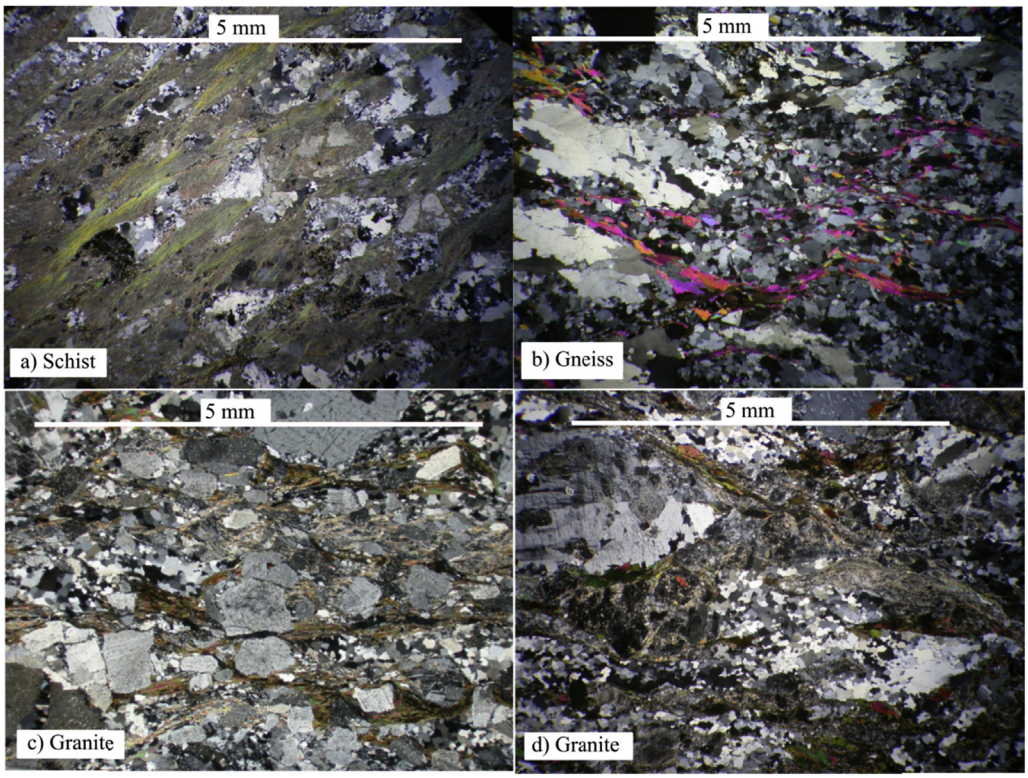

Fig. 2. Photomicrographs under plane-polarised light of lithologies in which penetration tests were conducted.

and the slope and the length of the curve beyond the critical thrust point are representative of the 100–200 mm thickness of rock over which the test is performed. Performing the test in different lithologies will produce different curves, which can be related back to the geological conditions.

The steady-state penetration rate is limited by TBM design parameters, which define performance limits. The penetration limit is a function of muck conveyance, bucket design, cutter wear and the maximum head revolution speed (Frenzel et al., 2012). The torque limit provides the transition from the penetration limit to the maximum thrust (Frenzel et al., 2008), which is a function of the rotational speed and is controlled by the maximum torque capacity. The thrust limit is controlled by cutter type, maximum thrust capacity and TBM head design. The penetration limit for the TBMs used in this investigation is approximately 11 mm/rev. The torque limit for the TBMs in this study is approximately 30% of the maximum torque capacity. The maximum net thrust on 432 mm cutters is typically around 250–267 kN (Frenzel et al., 2008; Maidl et al., 2008).

Poisel et al. (2010) suggested that TBM factors, such as vibration and driving style, have a major impact on the penetration rate within the same rock mass. The penetration-thrust graphs can only be used for interpretation of geological conditions if the assumption is made that the TBM is operated at one of the TBM limits. If the TBM is not operated at its limit, non-unique interpretations can be made, which are not necessarily related to geology. The steady-state stroke data in Fig. 11 show that in most cases, the TBM is operated near these limits to maximise production, so this issue is considered to be rare. While operational variations may have some impacts on penetration rates, if it is assumed that the TBM is operated near the upper limits, then geological variations, which have a fundamental impact on the efficiency of the chipping process, will control the penetration rate.

The data from penetration tests represent geological conditions over a very short tunnel length (hundreds of millimetres) but, in conjunction with steady-state stroke data, can be used to infer the geological conditions over several strokes, provided that the rock mass is homogeneous over this length. Conversely, the test results can be used to demonstrate changes in geological conditions and the impact of those changes on the cutting process. The steady-

Table 1
Performance indicators derived from steady-state data and penetration test data from Figs. 3–5, and intact rock strength.

Sample	Penetration index (kN (rev mm^{-1}))	Critical thrust (kN)	$I_{S(50)}$ (MPa)	UCS (MPa)	Distance from UCS test (m)
Schist 4	77	65	–	115	7
Schist 5	139	125	–	115	1
Schist 6	75	75	–	115	23
Schist 1	59	50	–	100	50
Schist 2	49	50	–	95	37
Schist 3	61	50	–	100	19
Granite 1	117	150	8	155	41
Granite 2	138	150	5	150	23
Granite 3	74	85	2	130	6
Granite 4	130	170	7	150	7
Granite 5	108	120	5	150	21
Granite 6	215	210	8	185	7
Granite 7	183	200	7	185	1
Gneiss 1	171	200	–	–	–
Gneiss 2	195	250	–	–	–
Gneiss 3	244	250	–	–	–
Granite T05 (Gong et al., 2007)	208	210	–	175	–
Marble 2 HT03 (Yin et al., 2014)	129	100	–	105	–
Marble 3 DT (Yin et al., 2014)	43	50	–	135	–

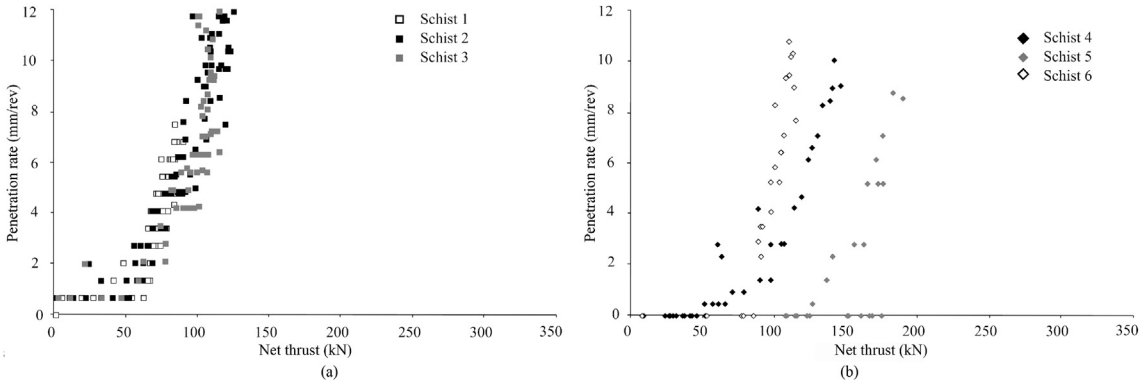

Fig. 3. Penetration test data for schist.

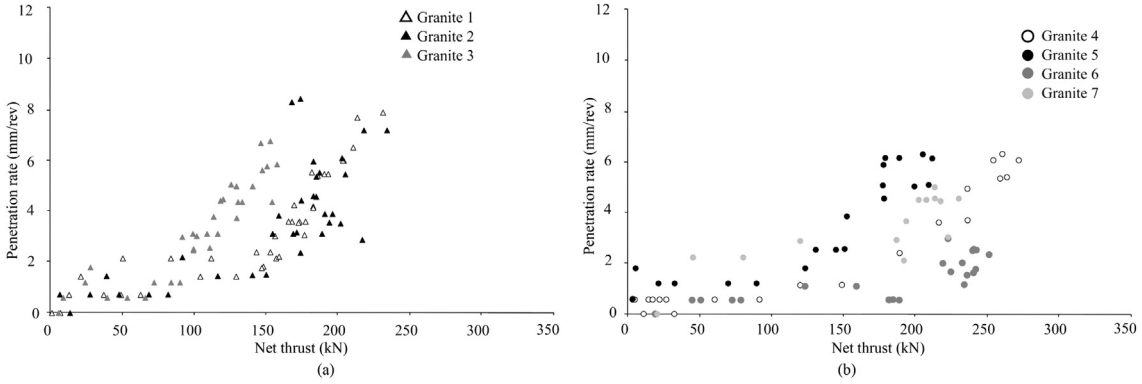

Fig. 4. Penetration test data for granite.

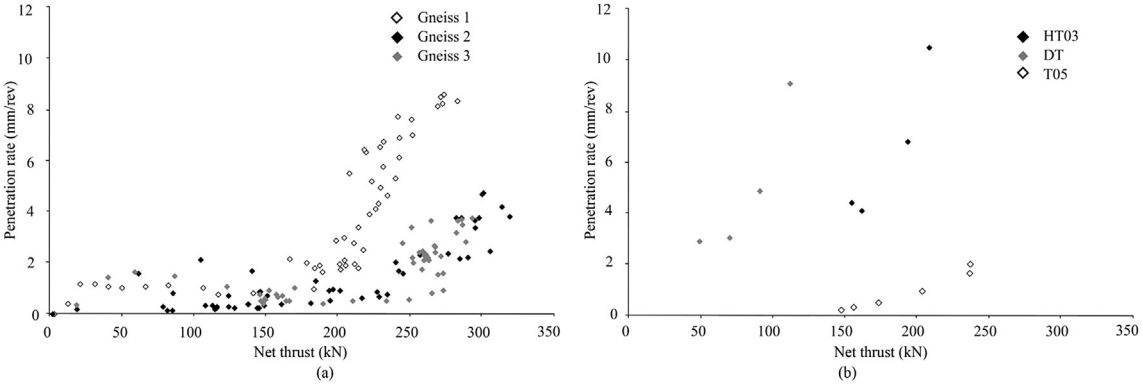

Fig. 5. Penetration test data for (a) gneiss, and (b) two marble samples (HT03 and DT) in Yin et al. (2014) and one granite sample (T05) in Gong et al. (2007).

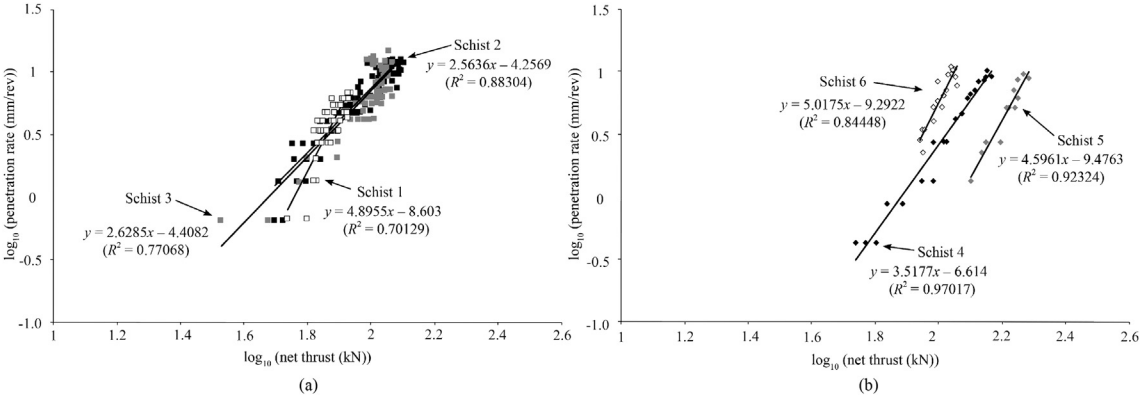

Fig. 6. Penetration test data plotted as common logarithms according to Bruland (1998) for schist.

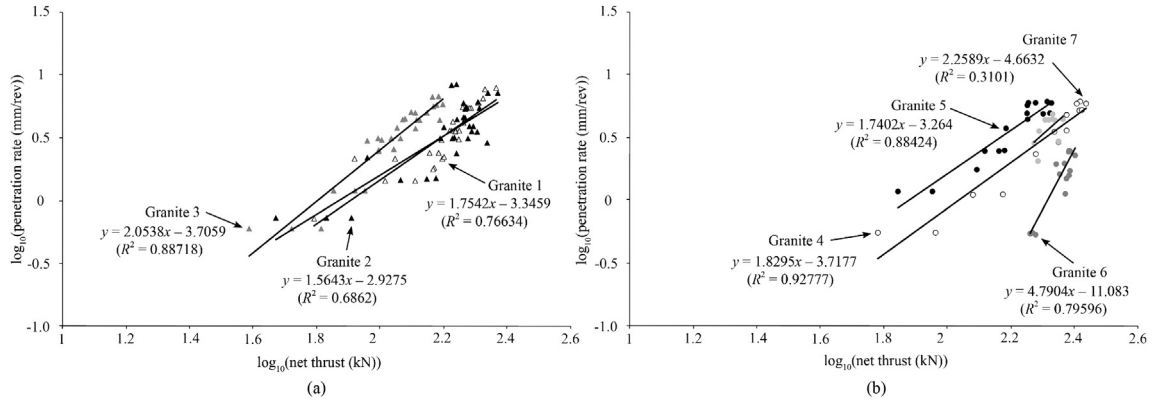

Fig. 7. Penetration test data plotted as common logarithms according to Bruland (1998) for granite.

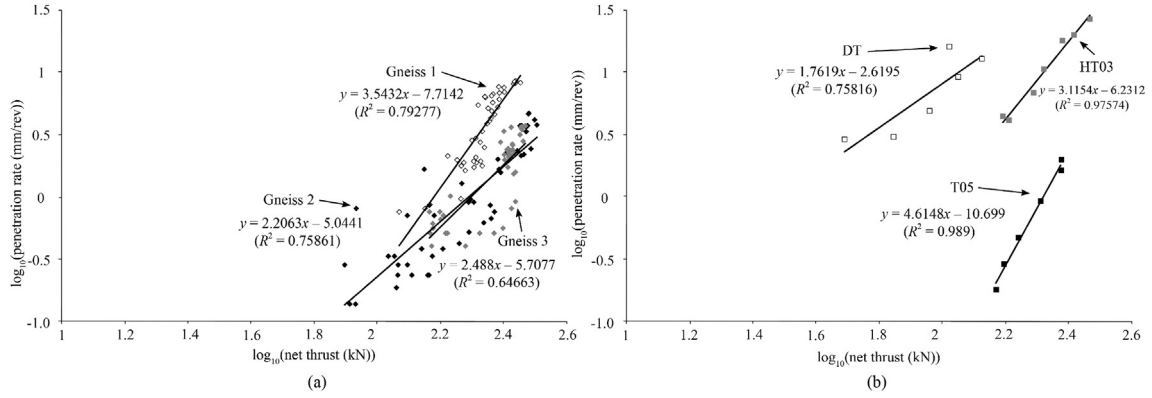

Fig. 8. Penetration test data plotted as common logarithms according to Bruland (1998) for (a) gneiss, and (b) two marble samples (HT03 and DT) tested in Yin et al. (2014) and one granite sample (T05) from Gong et al. (2007).

Table 2
Performance parameters derived from penetration test data from Figs. 6–10.

Sample	Penetration coefficient (A_R)	B_R	M_1 (kN)	*SMRBI* (kN (rev mm^{-1}))	$-c$
Schist 4	3.5177	6.6	76	77	0.724
Schist 5	4.5961	9.5	115	118	0.893
Schist 6	5.0175	9.3	71	75	0.832
Schist 1	4.8955	8.6	57	37	0.808
Schist 2	2.5636	4.3	46	33	0.646
Schist 3	2.6285	4.4	48	32	0.752
Granite 1	1.7542	3.3	81	55	0.702
Granite 2	1.5643	2.9	74	75	0.807
Granite 3	2.0538	3.7	64	47	0.634
Granite 4	1.8295	3.7	108	130	0.595
Granite 5	1.7402	3.3	75	82	0.668
Granite 6	4.7904	11.1	206	133	0.872
Granite 7	2.2589	4.7	116	132	0.896
Gneiss 1	3.5432	7.7	150	88	0.81
Gneiss 2	2.2063	5	193	177	0.668
Gneiss 3	2.488	5.7	197	174	0.9
Granite T05 (Gong et al., 2007)	4.6148	10.7	208	208	0.786
Marble 2 HT03 (Yin et al., 2014)	3.1154	6.2	100	110	0.709
Marble 3 DT (Yin et al., 2014)	1.7619	2.6	31	43	0.551

state stroke data can be used to derive the net specific penetration (net SP in Fig. 11), which is the ratio of penetration rate to thrust (in mm rev^{-1} kN^{-1}), per cutter (Farrokh et al., 2012). The net SP is the inverse of penetration index, and they can be used interchangeably depending on data analysis needs. Comparison of penetration index with critical thrust (Fig. 12) shows that rocks which change from grinding to chipping at high thrust (high critical thrust) will also tend to require high thrust per increment of penetration rate (high penetration index).

4.2. Logarithm penetration curves

Linear regression of common logarithm penetration curves provides a method for consistently obtaining measures of TBM excavation performance. The algorithm developed by Bruland (1998) is repeatable and relatively simple. The key parameter, M_1, provides a consistent measure for net thrust required to achieve a penetration rate value of 1 mm/rev. This threshold of 1 mm/rev is useful but arbitrary, and does not necessarily reflect the transition from grinding to chipping. The schist samples in Fig. 3 have transitioned to chipping by the time the penetration rate reaches 1 mm/rev, whereas Granites 5 and 7 (Fig. 4b) and Gneiss 1 (Fig. 5a) do not chip until the penetration rate is greater than 1 mm/rev. The fitting curve between M_1 and critical thrust (Fig. 12) shows a reasonable agreement with the test data, and that M_1 is typically 75% of the critical thrust. The values of A_R and M_1 obtained from Eq. (1) can be used to derive the fitting equation (Bruland, 1998):

$$i_0 = \left(\frac{M_t}{M_1}\right)^{A_R} \tag{3}$$

where M_t is the net thrust (kN) at any penetration rate i_0 (mm/rev). The fitting curves show good agreement with the test data (Fig. 13).

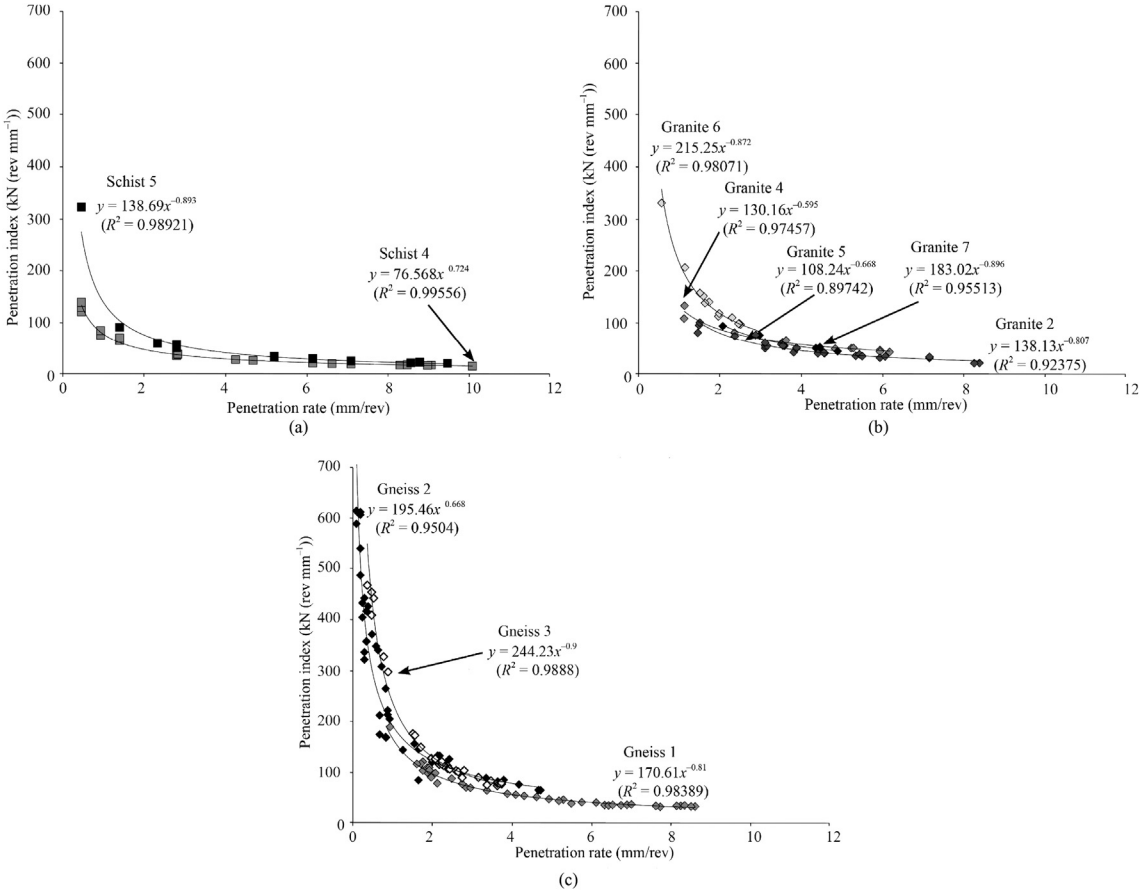

Fig. 9. Penetration test data plotted to determine *SRMBI* for stable face conditions.

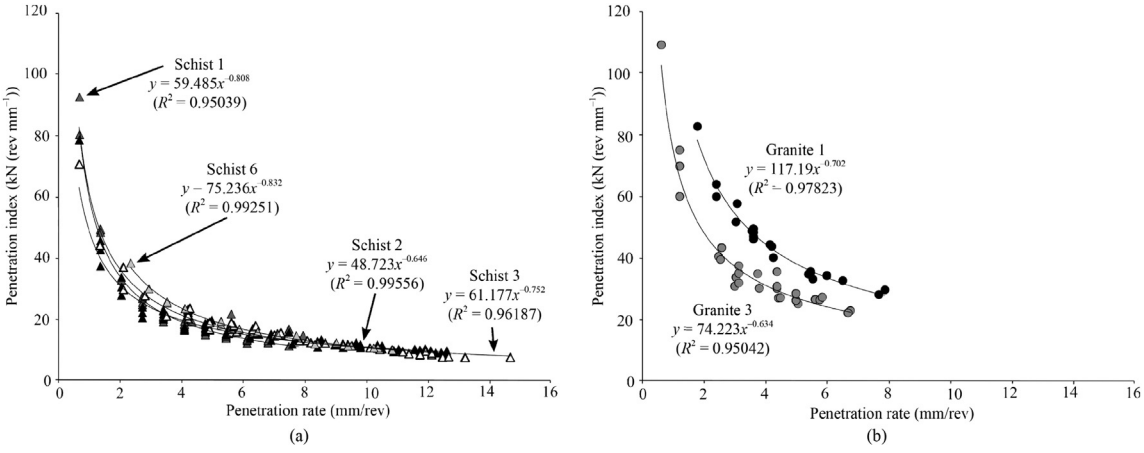

Fig. 10. Penetration test data plotted to determine *SRMBI* for unstable face conditions.

Power functions, such as Eq. (3), do not have inflection points. Since the critical thrust is defined as the inflection point in the penetration-thrust graph, processing penetration test data using Eq. (3) will not provide a value for the transition from grinding to chipping (for example the location of critical thrust for Gneiss 1 in Fig. 13a).

4.3. Penetration index curves

The penetration index curve provides a simple method for obtaining *SRMBI*, which does not depend on the machine operation conditions (thrust force, RPM and torque) and eliminates the influence of the operation uncertainties on the rock mass response to excavation (Gong et al., 2007; Gong and Zhao, 2009). The relationships between *SRMBI* values and penetration index, critical thrust and M_1 (Fig. 14) show that each of them has a reasonably good linear fit with the test data. The fitting curves between the critical thrust and M_1 have a slope approaching 1, whereas that of penetration index does not. The fitting between *SRMBI* and the critical thrust is better than those of M_1 and penetration index (Fig. 12).

4.4. Discussion

M_1 and *SRMBI* are both directly derived from penetration test data and provide a measure of performance for the arbitrary

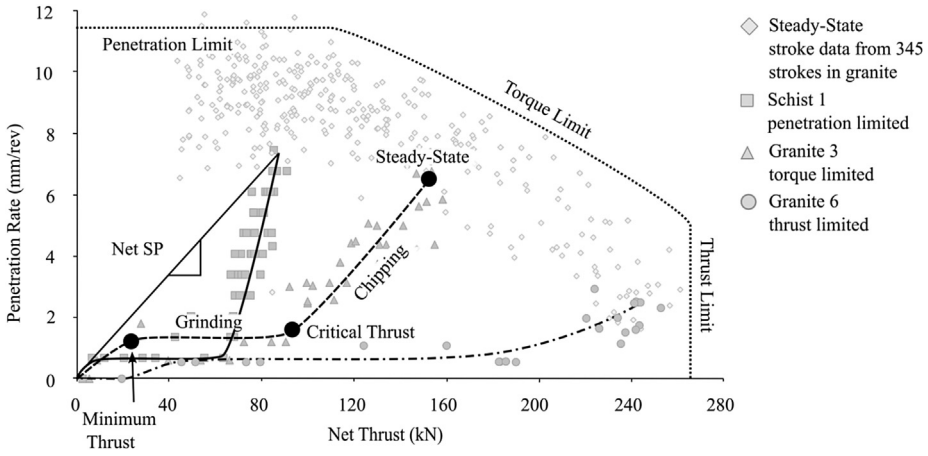

Fig. 11. Penetration test data showing the key components of the curve.

penetration rate threshold of 1 mm/rev. The penetration graphs in Figs. 3–5 show that the transition from grinding to chipping does not consistently occur at 1 mm/rev. While M_1 and *SRMBI* are obtained using objective formulas (i.e. Eqs. (1) and (2), respectively), manual analysis is required to determine the inflection point for critical thrust. Depending on the quality of the penetration test data, in particular the density of data points defining the start-up curve, it is not always possible to identify the critical thrust (e.g. Fig. 5b). For this reason, a precision of 5 kN was selected for critical thrust for the tests in this study, and in Yin et al. (2014) and Gong et al. (2007). Considering the ease with which the critical thrust can be obtained with good penetration test data, however, if the goal of the penetration test is to identify the transition to chipping, the critical thrust is preferable to M_1 or *SRMBI*. If the goal of the penetration test is to generate objective performance data at a penetration rate of 1 mm/rev (e.g. for contract purposes), then the formulation-based performance indicators M_1 or *SRMBI* may be preferred.

The penetration curves can be fit using Eq. (3), providing a means to interpolate or extrapolate from test data (Schist 4 in Fig. 13a and the tests shown in Fig. 13b). The fits can underestimate the penetration rate at low (Gneiss 1 and 2 in Fig. 13a) and very high (Gneiss 2 in Fig. 13a) thrusts, and do not provide an indication of the transition from grinding to chipping as clearly as visual inspection of the raw data (e.g. Gneiss 1 in Fig. 13a).

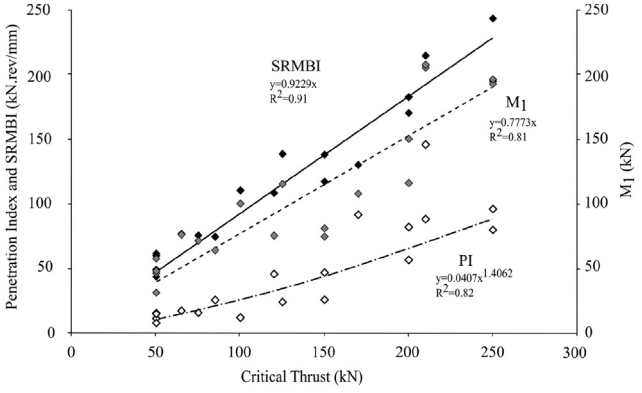

Fig. 12. Comparison of performance indicators derived from penetration tests in this study, and those in Yin et al. (2014) and Gong et al. (2007).

5. Penetration curves as indicators of excavation performance

The UCS values for the schist and granite in which the penetration tests were conducted show a strong relationship with critical thrust (Fig. 15), penetration index, as observed by Alber (2008) and Hassanpour et al. (2011, 2015), and *SRMBI*, as observed by Gong et al. (2007) and Yin et al. (2014). The variance in these relationships likely results from fractures (pre-existing or stress-induced)

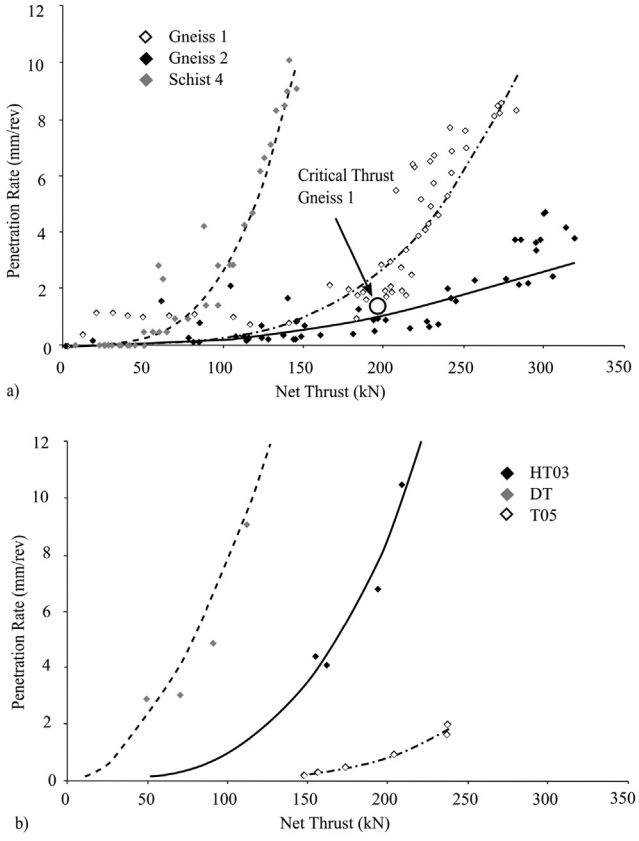

Fig. 13. Penetration test data for (a) Schist 4, Gneiss 1 and Gneiss 2, and (b) two marble samples (HT03 and DT) tested in Yin et al. (2014) and one granite sample (T05) from Gong et al. (2007), showing the data fits obtained using Eq. (3).

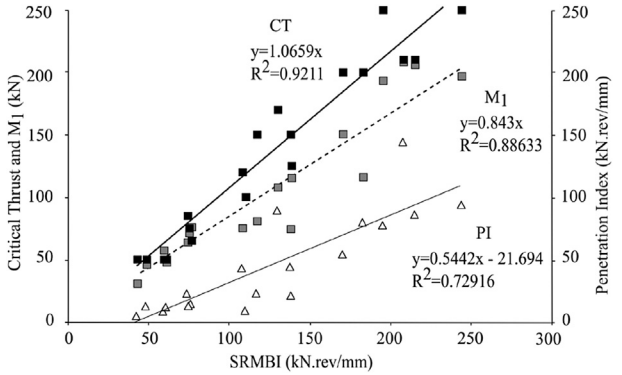

Fig. 14. Relationships between penetration index, M_1 and critical thrust and *SRMBI* obtained from penetration tests in this study and in Yin et al. (2014) and Gong et al. (2007). CT represents the critical thrust.

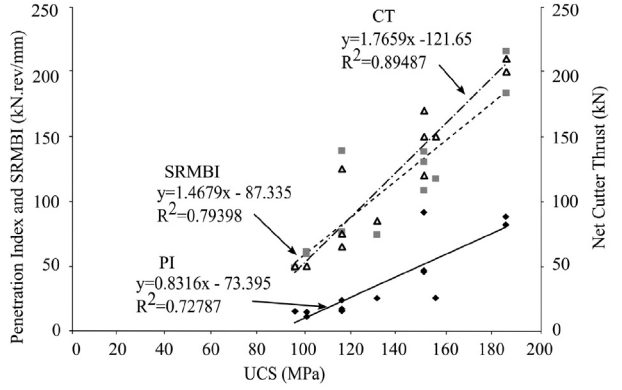

Fig. 15. Comparison of UCS versus performance indicators from penetration tests in schist and granite.

in the face. The relationships between UCS and penetration index and *SRMBI* have greater variances than that for critical thrust. The critical thrust and *SRMBI* have nearly the same relationship with UCS, as shown in Fig. 15. Rock mass characteristics have been shown to have an impact on penetration index (Sapigni et al., 2002; Hassanpour et al., 2015), possibly to a greater extent than the critical thrust, contributing to this greater variance.

The penetration curves under stable face conditions in the schist, gneiss and granite are grouped in Fig. 16 according to the dominant excavation mode. The curves for Schists 4 and 5 have the lowest strength (115 MPa) and a critical thrust less than 100 kN, and the rocks change to chipping-dominated excavation effectively. Schist 4, in particular, demonstrates high excavation performance near the penetration limit. The curves for Granites 2, 5 and 7 have moderate strength between 150 and 185 MPa and tend to have a critical thrust between 100 kN and 200 kN (Fig. 16). The curves above the critical thrust are torque limited and tend to be moderately long and steep, showing that chipping was occurring, but not very efficiently. In these rock masses, the high thrust will cause deep indentation, but the mixed tensile-shear fracturing process in the kerf will lead to high rolling forces and high torque (Yin et al., 2014) without generating chips effectively.

The curves with critical thrust above 200 kN (Granites 4 and 6, T05, and Gneiss 2 and 3 in Fig. 16) are very short with shallow slope, and are limited by the cutter thrust. The high critical thrust shows that minimal chipping is occurring due to high UCSs (150 MPa, 185 MPa and 175 MPa for Granite 4, Granite 6 and T05, respectively), resulting in excavation dominated by the very inefficient grinding process. More importantly, the penetration rate for these high strength rocks will be dependent on their ability to propagate fractures. The critical thrust is very close to the cutter thrust limit and the short shallow curve above the critical thrust shows that fracture propagation is not occurring efficiently once it has been initiated. This shallow curve above the high critical thrust demonstrates that, for penetration to occur, a considerable increase in thrust is required, which is very energy intensive.

The critical thrust and the slope of the penetration curve above the critical thrust are the key indicators of cutter efficiency, which are controlled by the strength (Fig. 17) and ease of fracture propagation and coalescence once new fractures have been initiated. Geological characteristics play an important role in both the strength and the ability to propagate fractures. An easy transition to tensile fracturing processes (chipping) occurs in Schist 4, which has a well-defined micaceous (40%) cleavage that facilitates fracture propagation (Villeneuve et al., 2012). A less efficient transition to tensile fracturing with some shear fracturing, and thus less chipping, occurs in Granite 2, which has a poorly defined micaceous

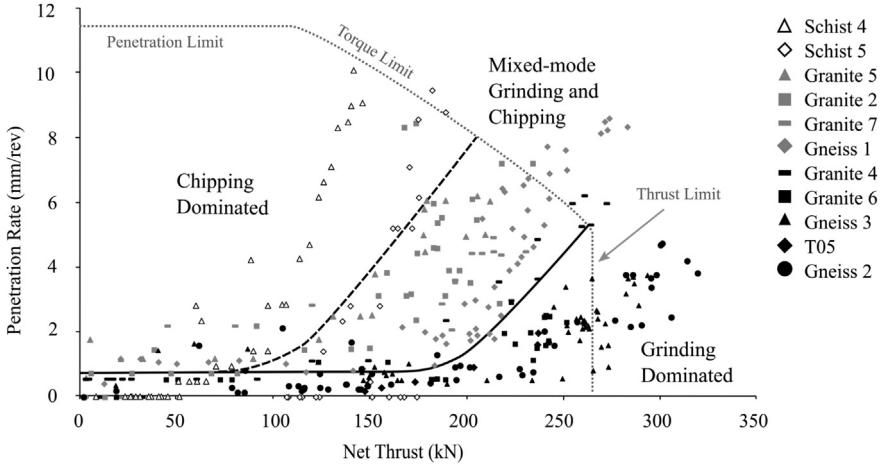

Fig. 16. Penetration curves for schist, granite and gneiss samples from this study and one granite sample from Gong et al. (2007) excavated under stable face conditions overlaid by the performance limits from Fig. 11.

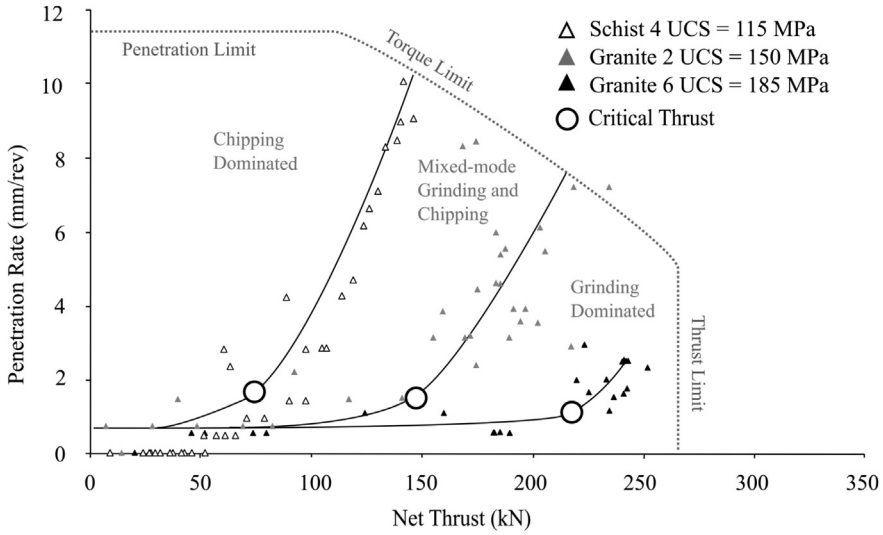

Fig. 17. Penetration curves for selected schist and granite samples under stable face conditions showing the location of critical thrust overlaid by the performance limits from Fig. 11, and excavation types from Fig. 16.

(15%) schistocity. Shear-dominated fracturing (grinding) occurs in Granite 6, which has very low mica content (5%) and no foliation.

As demonstrated by Granites 2 and 6, geological characteristics, such as fabric and mica content, are especially important for rocks with moderate to high critical thrust, where the ability to propagate fractures can make a large difference in the resulting penetration rate (i.e. torque limited rather than thrust limited). This may also account for some of the variances in the relationships between UCS and penetration index and *SRMBI* in Fig. 15.

These findings can be used to provide guidance to aid in drawing up contract documents and selecting method by which TBM performance will be used for payment and progress assessment, depending on the anticipated geomechanical and geological conditions. During construction, penetration tests can be used to provide guidance to TBM operators regarding thrust application. In a rock type similar to Granite 6, which tends to be excavated via the grinding process, very little gain in penetration rate can be achieved by applying higher thrust, and wear and cutter damage could be minimised by lowering the thrust without substantially reducing the penetration rate. Chipping-dominated excavation may never be achieved in these rock types with very high strength, even if cutter thrust limits were increased, as the process will remain too energy intensive due to the high fracture initiation threshold and the poor fracture propagation in these rocks.

6. Penetration curves as indicators of stress-induced face instability

A selection of penetration curves for tests under unstable (stress-induced) and stable face conditions in the schist and granite is shown in Fig. 18, again overlain by lines highlighting the dominant excavation mode. The two schist samples have the same UCS (115 MPa), similar to that of the granites (155–150 MPa). Stress-induced face instability improves the penetration rate, in these two cases by 14% and 19%, respectively, making it easier to generate chips or creating larger blocks (Gong et al., 2012). These measures do not capture the negative impacts of stress-induced face instability on TBM performance, which has been previously discussed (Villeneuve, 2008; Gong et al., 2012; Yin et al., 2014).

By plotting the penetration coefficient and M_1 values derived using Eq. (1), it is possible to identify whether the penetration is affected by face instability (Fig. 19). The data cluster according to face stability and whether the excavation is grinding- or chipping-dominated, both for the dataset from this study in schist, granite and gneiss, and for the data from marble in Yin et al. (2014) and from granite in Gong et al. (2007). A line with a slope of 20° separates the penetration tests where there was stress-induced face instability from the rest of the data. In addition, a slope of 45° separates the tests where the excavation was grinding-dominated from the rest of the data. The data that fall between these lines are transitional data. These tests were conducted either in rocks with mixed-mode grinding and chipping, or in areas with slight to moderate face instability, or in a combination of both.

Villeneuve (2008) and Villeneuve et al. (2012) showed that mineralogy is important for tensile-dominated fracturing. In particular, they found that rocks with low (<10%) and high (>24%) mica contents are not as sensitive to tensile-dominated fracturing and spalling as those with moderate mica content. In the case of low mica content, because there are few fracture initiators in the form of mica grains, mica can also act as a fracture inhibitor. In the case of high mica content, fractures may be initiated, but will not propagate well, reducing the potential for spalling. It was also shown that the ratio between quartz content and feldspar content is important for tensile-dominated fracturing and spalling. A higher quartz to feldspar ratio reduces the potential for spalling because quartz is neither a good fracture initiator nor a good fracture propagator.

Granite 1 is an example of transition rock, where the intact rock strength is high, but its geological characteristics, in particular, its micaceous schistosity, 16% mica content, 30% quartz content, and quartz to feldspar ratio of 0.5, make it more sensitive to spalling than Granite 4 (10% mica, poorly defined cleavage, 30% quartz content, and quartz to feldspar ratio of 0.5), leading to moderate stress-induced face instability. Schist 5 is also a transition rock in this case due to its lower strength, high mica content (40%), and high quartz (35%) to feldspar ratio (1.3), which lead to mixed-mode chipping and grinding, but little stress-induced face instability. The mica content (25%) and quartz (35%) to feldspar ratio (1) in Schist 6 are lower, leading to moderate stress-induced face instability.

Determination of M_1 and penetration coefficient is useful for identifying not only the critical net thrust at 1 mm/rev as an objective measure of performance, but also rock masses in which

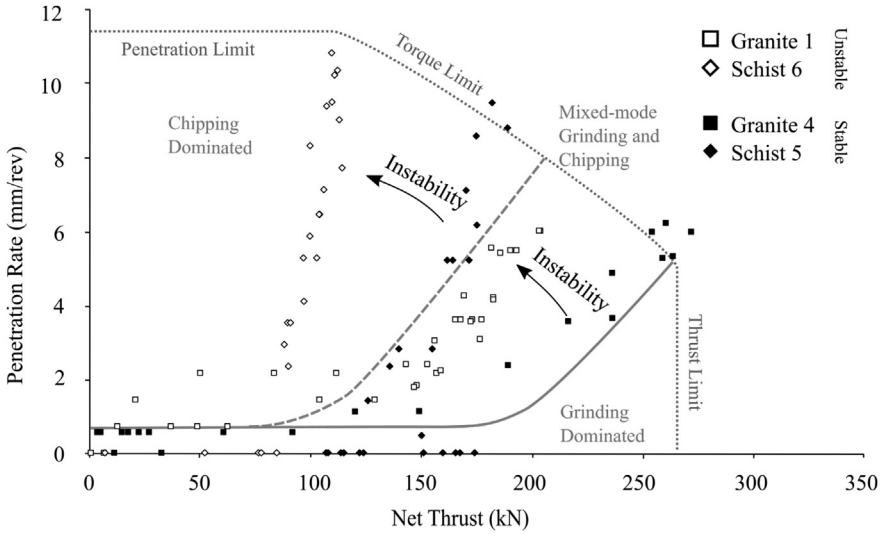

Fig. 18. Penetration curves for selected schist and granite samples under stable and unstable face conditions compared to the performance curves from Fig. 11, and excavation types from Fig. 16.

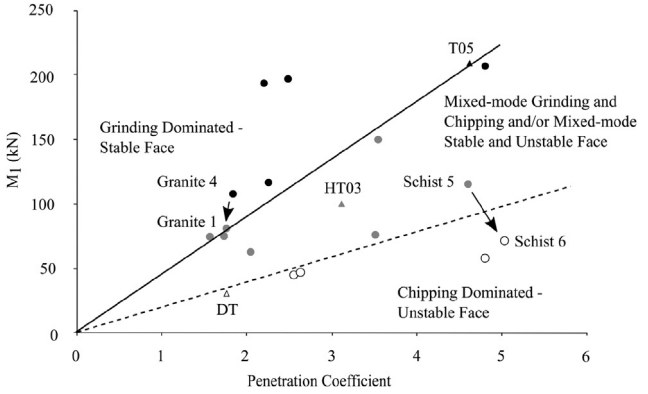

Fig. 19. Comparison of M_1 obtained using Eq. (1) for schist and granite samples from this study, two marble samples from Yin et al. (2014), and one granite sample from Gong et al. (2007), showing boundaries associated with chipping performance and face stability. The solid line corresponds to a slope of 45° and the dashed line to a slope of 20°.

grinding is dominant, or stress-induced face instability is affecting the penetration rate. This approach can help TBM operators identify rock masses in which additional thrust will not lead to large improvement in performance. It can also provide a contractual method to identify rock masses that are being affected by stress-induced face instability.

7. Conclusions

This research focused on the determination of the impact of intact rock characteristics at the tunnel face on the rock cutting process. It was demonstrated that TBM penetration tests can provide a large range of measures of TBM performance. It was illustrated that M_1 and *SRMBI*, which provide information about the thrust required to achieve a penetration rate of 1 mm/rev, and the critical thrust, the thrust required to transition from grinding to chipping, are not equivalent measures, but are correlated. M_1 and *SRMBI* are easily obtained objective measures of TBM performance. Critical thrust, which requires to be input by users and is thus more difficult to be obtained, can provide an understanding of the transition from grinding to chipping, while M_1 and *SRMBI* cannot.

Penetration test data and average stroke running data were used to categorise penetration-thrust graphs according to TBM operational constraints and excavation performance from grinding-dominated, through mixed-mode grinding and chipping, to chipping-dominated mode. Using these categorised graphs, it was shown that rocks with higher strength tend to be excavated through the grinding-dominated process. For massive rock masses with significantly high strength, over 175 MPa in this study, only minor gains in penetration rate can be achieved through increased thrust application because the critical thrust approaches the cutter thrust limit of 267 kN for commonly used 432 mm (17 in) cutters. Penetration testing can help TBM operators identify whether additional thrust is warranted in individual rock masses with low penetration rates during excavation.

Penetration tests, along with visual observation of the tunnel face and muck, can also help to identify stress-induced face instability. It was shown that stress-induced face instability leads to increased penetration rates, although any other effects of the instability on TBM utilisation were not discussed. A method was proposed for clearly identifying stress-induced face instability using M_1 and penetration coefficient parameters derived from penetration test data. A ratio between M_1 and the penetration coefficient above 45 would suggest that rock masses are excavated through grinding-dominated processes. A ratio below 20 would suggest that rock masses are experiencing stress-induced face instability. A ratio between 20 and 45 suggests that rock masses are excavated by mixed-mode of grinding and chipping, experiencing slight to moderate stress-induced face instability, or a combination of the two modes.

Finally, we have shown that geological characteristics, in addition to rock strength, play an important role in both the chipping process and stress-induced face instability. Under similar stress conditions, rocks with well-defined fabric, oriented oblique to the tunnel face, were easier to be excavated and were more sensitive to stress-induced face instability than rocks without fabric or fabric oriented perpendicular to the face. Rocks with very high mica content were easier to be excavated, but were less sensitive to stress-induced face instability than rocks with a moderate mica content.

The penetration test methodology can be used for further investigation into the rock cutting process, to aid in developing better penetration rate prediction tools, and as a measure of TBM performance for tunnelling contract management during excavation. We have shown that our methodologies provide repeatable results using data from Gong et al. (2007) and Yin et al. (2014). For these data to be comparable across projects, a consistent testing methodology should be used, for example, the methodology proposed in Gong et al. (2007) or Frenzel et al. (2012).

Conflict of interest

The author wishes to confirm that there are no known conflicts of interest associated with this publication and there has been no significant financial support for this work that could have influenced its outcome.

Acknowledgements

This work was supported by Herrenknecht AG, a Postgraduate Scholarship from the Natural Science and Engineering Research Council (NSERC) of Canada and the Golder Associates (Canada) Visitor Programme to the Queen's Geo-Engineering Centre. Murer-Strabag and Tunnel Alp Transit consortia are also thanked for their in-kind support during penetration testing and data collection. The scientific supervisors of this research are also acknowledged for their tremendous support.

References

Alber M. An integrated approach to penetration, advance rates and disc cutter wear for hard rock TBM drives. Geomechanics and Tunnelling 2008;1(1):29–37.
Barton N. TBM tunnelling in jointed and faulted rock. Rotterdam: A.A. Balkema; 2000.
Bieniawski ZT, Celada Tamames B, Galera Fernández JM, Álvarez Hernández M. Rock mass excavability indicator: new way to selecting the optimum tunnel construction method. Tunnelling and Underground Space Technology 2006;21(3–4):237.
Bruland A. Hard rock tunnel boring design and construction. Trondheim, Norway: Norwegian University of Science and Technology; 1998.
Cigla M, Yagiz S, Ozdemir L. Application of tunnel boring machines in underground mine development. In: Proceedings of the 17th international mining congress and exhibition of Turkey. Ankara, Turkey; 2001. p. 155–64.
Farrokh E, Rostami J, Laughton C. Study of various models for estimation of penetration rate of hard rock TBMs. Tunnelling and Underground Space Technology 2012;30:110–23.
Frenzel C, Galler R, Käsling H, Villeneuve M. Penetration tests for TBMs and their practical application. Geomechanics and Tunnelling 2012;5(5):557–66.
Frenzel C, Käsling H, Thuro K. Factors influencing disc cutter wear. Geomechanics and Tunnelling 2008;1(1):55–60.
Gehring K. The influence of TBM design and machine features on performance and tool wear in rock. Geomechanics and Tunnelling 2009;2(2):140–55.
Gertsch R, Gertsch L, Rostami J. Disc cutting tests in Colorado Red Granite: implications for TBM performance prediction. International Journal of Rock Mechanics and Mining Sciences 2007;44(2):238–46.
Gong QM, Zhao J, Jiang YS. In situ TBM penetration tests and rock mass boreability analysis in hard rock tunnels. Tunnelling and Underground Space Technology 2007;22(3):303–16.
Gong QM, Zhao J. Development of a rock mass characteristics model for TBM penetration rate prediction. International Journal of Rock Mechanics and Mining Sciences 2009;46(1):8–18.
Gong QM, Yin LJ, Wu SY, Zhao J, Ting Y. Rock burst and slabbing failure and its influence on TBM excavation at headrace tunnels in Jinping II hydropower station. Engineering Geology 2012;124:98–108.
Hassanpour J, Rostami J, Zhao J. A new hard rock TBM performance prediction model for project planning. Tunnelling and Underground Space Technology 2011;26(5):595–603.
Hassanpour J, Rostami J, Zhao J, Azali S. TBM performance and disc cutter wear prediction based on ten years experience of TBM tunnelling in Iran. Geomechanics and Tunnelling 2015;8(3):239–47.
Maidl B, Schmid L, Ritz W, Herrenknecht M. Hardrock tunnel boring machines. Berlin: Ersnt & Sohn Verlag; 2008.
Poisel R, Tentschert E, Preh A, Ostermann V, Chwatal W, Zettler A. The interaction of machine and rock mass analysed using TBM data and rock mass parameters. Geomechanics and Tunnelling 2010;3(5):510–9.
Robbins RJ. Economic factors in tunnel boring. In: Proceedings of the South African tunnelling conference: the technology and potential of tunnelling, vol. 1. Johannesburg; 1970. p. 217–21.
Rostami J, Gertsch R, Gertsch L. Rock fragmentation by disc cutter: a critical review and an update. In: Hammah R, Bawden W, Curran J, Telesnicki M, editors. Mining and tunnelling innovation and opportunity, proceedings of the 5th North American rock mechanics symposium and 17th tunnelling association of Canada conference. Toronto, Canada: University of Toronto Press; 2002.
Samuel AE, Seow LP. Disc force measurement on a full-face tunnelling machine. International Journal of Rock Mechanics and Mining Sciences & Geomechanics Abstracts 1984;21(2):83–96.
Sapigni M, Berti M, Behtaz E, Busillo A, Cardone G. TBM performance estimation using rock mass classification. International Journal of Rock Mechanics and Mining Sciences 2002;39(6):771–88.
Snowdon RA, Ryley MD, Temporal J. A study of disc cutting in selected British rocks. International Journal of Rock Mechanics and Mining Sciences & Geomechanics Abstracts 1982;19(3):107–21.
Teale R. The mechanical excavation of rock – experiments with roller cutters. International Journal of Rock Mechanics and Mining Sciences & Geomechanics Abstracts 1964;1(1):63–78.
Villeneuve MC, Diederichs MS, Kaiser PK, Frenzel C. Geomechanical characterisation of massive rock for deep TBM tunnelling. In: Eberhardt E, Stead D, Morrison T, editors. Rock mechanics: meeting Society's challenges and demands, proceedings of the 1st Canada-US rock mechanics symposium. CRC Press; 2007. p. 1131–9.
Villeneuve MC. Examination of geological influence on machine excavation of highly stressed tunnels in massive hard rock [PhD thesis]. Kingston, Canada: Queen's University; 2008.
Villeneuve MC, Diederichs MS, Kaiser PK. Effects of grain scale heterogeneity on rock strength and the chipping process. International Journal of Geomechanics 2012;12(6):632–47.
Yin LJ, Gong QM, Zhao J. Study on rock mass boreability by TBM penetration test under different in situ stress conditions. Tunnelling and Underground Space Technology 2014;43:413–25.
Zhang Z. Laboratory studies of dynamic rock fracture and in-situ measurements of cutter forces for a boring machine [PhD thesis]. Luleå, Sweden: Luleå University of Technology; 2001.
Zhang ZX, Kou SQ, Tan XC, Lindqvist PA. In-situ measurement of cutter forces on boring machine at Äspö Hard Rock Laboratory. Part I. Laboratory calibration and in-situ measurements. Rock Mechanics and Rock Engineering 2003;36(1):39–61.

Dr. Marlène Villeneuve is a Senior Lecturer at the University of Canterbury. Her role includes teaching, supervising postgraduate students and conducting research. Her research focuses on testing and characterisation of intact rock and rock masses as well as numerical modelling of rock fracturing processes for tunnelling, drilling and slope stability. These geomechanical techniques are aimed at finding relationships between geological characteristics and the current physical and mechanical properties of rocks. These techniques, whether in the laboratory, the field or the computer laboratory, are applied to researches for a variety of industries, including tunnelling, slope stability, drilling, geothermal energy, volcanology, and petroleum resources. This requires working closely with geologists and engineers, and providing the link between the two disciplines. Dr. Villeneuve has experience with geotechnical and geological site characterisations, static and seismic slope and excavation stability analyses, tunnel support and initial lining design, tunnel construction inspection, TBM excavation and numerical modelling. While working in industry, she produced contract drawings, construction specifications, calculations, design reports, and numerous technical memoranda. Since returning to academia, she has produced several research papers, supervised over 15 postgraduate students and has been involved with national (New Zealand Geotechnical Society) and international (International Society of Engineering Geologists) professional societies.